Adaptive fully implicit multi-scale finite-volume method for multi-phase flow and transport in heterogeneous porous media

P. Jenny [a], S.H. Lee [b], H.A. Tchelepi [c],*

[a] *Institute of Fluid Dynamics, ETH, Zurich, Switzerland*
[b] *Chevron Energy Technology Company, San Ramon, CA 94583, USA*
[c] *Petroleum Engineering Department, Stanford University, 367 Panama Street, Green Earth Sciences Building, Rm 065, Stanford, CA 94305, USA*

Abstract

We describe a sequential fully implicit (SFI) multi-scale finite volume (MSFV) algorithm for nonlinear multi-phase flow and transport in heterogeneous porous media. The method extends the recently developed multiscale approach, which is based on an IMPES (IMplicit Pressure, Explicit Saturation) scheme [P. Jenny, S.H. Lee, H.A. Tchelepi, Adaptive multi-scale finite volume method for multi-phase flow and transport, Multiscale, Model. Simul. 3 (2005) 50–64]. That previous method was tested extensively and with a series of difficult test cases, where it was clearly demonstrated that the multiscale results are in excellent agreement with reference fine-scale solutions and that the computational efficiency of the MSFV algorithm is much higher than that of standard reservoir simulators. However, the level of detail and range of property variability included in reservoir characterization models continues to grow. For such models, the explicit treatment of the transport problem (i.e. saturation equations) in the IMPES-based multiscale method imposes severe restrictions on the time step size, and that can become the major computational bottleneck. Here we show how this problem is resolved with our sequential fully implicit (SFI) MSFV algorithm. Simulations of large (million cells) and highly heterogeneous problems show that the results obtained with the implicit multi-scale method are in excellent agreement with reference fine-scale solutions. Moreover, we demonstrate the robustness of the coupling scheme for nonlinear flow and transport, and we show that the MSFV algorithm offers great gains in computational efficiency compared to standard reservoir simulation methods.
© 2006 Elsevier Inc. All rights reserved.

Keywords: Numerical simulation; Multiscale methods; Finite-volume; Coupled flow and transport; Heterogeneous porous media; Immiscible multi-phase flow

* Corresponding author. Tel.: +1 650 723 9476.
  E-mail address: tchelepi@stanford.edu (H.A. Tchelepi).

1. Introduction

The level of detail in reservoir characterization models continues to grow. This is driven by the need to improve the predictive capacity of dynamic simulations of the complex reservoir displacement processes of practical interest. These highly detailed heterogeneous reservoir descriptions exceed the computational capability of existing reservoir simulators. This resolution gap is usually tackled by upscaling the fine-scale description to sizes that can be treated by the numerical simulator. In upscaling, the original model is coarsened using a computationally inexpensive process. In purely local flow-based upscaling methods [2,3], the process is usually based on single-phase flow. The simulation study of the multi-phase reservoir displacement process of interest is then performed using the coarsened (upscaled) model, which is derived using a simple flow process. These upscaling methods have proved quite successful. However, it is not possible to have a priori estimates of the errors that are present when complex flow processes are modeled using coarse models constructed via simplified settings.

The multiscale character of the properties of natural porous media makes the problem of predicting flow and transport in such systems a natural target for multiscale methods. As opposed to conventional upscaling techniques, we are interested in multiscale formulations that target the coupled problem of flow and transport with the original (fine-grid) description. The methodology is based on resolving the length and time scales of interest by maximizing local operations. Recent advances in this area show great promise. Gautier et al. [4] presented an approach for fast simulation of both flow and transport in heterogeneous porous media. They used nested grids to obtain the fine-grid flow field, and they integrated the saturation equation (i.e. the transport problem) along streamlines. Hou and Wu [5] developed a multiscale finite-element (MSFE) method, in which they constructed basis functions designed specifically to capture the fine-scale effects. In their approach, they achieved localization by boundary condition assumptions on the coarse elements. Hou and Wu [5] demonstrated both the accuracy and superior computational efficiency of their MSFE method compared to standard finite-element solutions of the fine-grid description. Their MSFE method, however, did not guarantee a locally conservative reconstruction of the fine-scale velocity field. Chen and Hou [6] extended the applicability of the multiscale framework by developing a method based on a mixed finite-element formulation. They provide clear evidence that a locally conservative fine-scale velocity field is necessary in order to perform accurate transport computations, even for single-phase flow of a tracer. Arbogast [7] and Arbogast and Bryant [8] presented a mixed finite-element method for nonlinear two-phase flow and transport in heterogeneous porous media. They localized the problems on the coarse elements using a special boundary condition assumption. Numerical Greens functions are used to account for the fine-scale effects on the coarse-scale solutions. Aarnes [9] proposed a modified mixed finite-element framework for modeling the flow problem in highly heterogeneous formations. His locally conservative method is based on the construction of special basis functions that are sensitive to the nature of the elliptic operator. Moreover, the construction accounts for radial flow in the vicinity of wells without resorting to complicated well models or near-well upscaling procedures.

Jenny et al. [10] developed a multi-scale formulation for the flow problem (pressure and total-velocity) that fits nicely into a finite-volume framework. In that multi-scale finite-volume (MSFV) method, one set of basis functions is used to obtain effective coarse-scale transmissibilities, and a second set of basis functions is devised to ensure that the reconstructed fine-scale total-velocity field is conservative. More recently, Jenny et al. [1] developed an adaptive sequential approach for multi-phase flow and transport. In their solution algorithm, the fine-scale flow field is obtained using the MSFV method, and an explicit scheme is then used to solve the saturation equation on the fine-scale description. This coupling approach is referred to as IMPES (IMplicit Pressure, Explicit Saturations) in the reservoir simulation community. The high accuracy and efficiency of this IMPES based MSFV method [1] was demonstrated for a wide variety of difficult heterogeneous test cases.

There has been a concerted effort to build highly detailed reservoir characterization models that represent the complex multiscale heterogeneity of natural geologic formations as accurately as possible. These high-resolution reservoir description models are thought to be more suitable for making predictions of reservoir flow performance. For such models, the ability to reconstruct high fidelity flow fields using a locally conservative multiscale scheme offers a huge computational advantage. However, the explicit treatment of the transport problem (i.e. saturation equations), which is employed in the IMPES-based MSFV method, imposes severe restrictions on the time step size. This can become the major computational bottleneck when solving highly

detailed heterogeneous problems of practical interest. Here we show how this problem is resolved with our Sequential Fully Implicit (SFI) MSFV algorithm. Although no attempts have been made to optimize the implementation, numerical experiments show that the method is highly efficient, and that the implicit MSFV results are in excellent agreement with reference fine-scale solutions.

The paper is organized as follows. In Section 2, the governing equations of the model problem are introduced. In Section 3, the fully implicit MSFV method for multi-phase flow and transport is described, and in Section 4, numerical studies are presented. Finally, conclusions are given in Section 5.

2. Immiscible two-phase flow and transport

We consider the case of immiscible two-phase (oil and water) flow in a heterogeneous porous medium. For incompressible fluids and rock, the conservation equations of the water and oil can be written as:

$$\phi \frac{\partial S_w}{\partial t} + \nabla \cdot \mathbf{u}_w = -q_w,$$
$$\phi \frac{\partial S_o}{\partial t} + \nabla \cdot \mathbf{u}_o = -q_o, \tag{1}$$

where ϕ is the porosity (ratio of pore to bulk volumes). In Eq. (1), S_j, $\mathbf{u}_j$, and q_j denote, respectively, the saturation, Darcy velocity and source term of fluid phase j, where j = w, o for water and oil. For our problem, the viscosities of the oil and water phases can be different, but the viscosity of each phase is constant. We also assume that capillarity and gravity effects are negligible; as a result, the Darcy velocities of the oil and water phases can be written as

$$\mathbf{u}_w = -\lambda_w \nabla p,$$
$$\mathbf{u}_o = -\lambda_o \nabla p, \tag{2}$$

where p is the pressure. The phase mobilities λ_w and λ_o are given by

$$\lambda_w = k(\mathbf{x}) \frac{k_{r_w}(S(\mathbf{x},t))}{\mu_w},$$
$$\lambda_o = k(\mathbf{x}) \frac{k_{r_o}(S(\mathbf{x},t))}{\mu_o}. \tag{3}$$

Here, k is the (absolute) permeability of the porous medium, k_{r_w} and k_{r_o} are the relative permeability functions of the oil and water phases, and μ_w and μ_o are the water and oil viscosities. The spatial distribution of the permeability is a dominant factor in dictating the flow behaviors in natural porous formations. The heterogeneity of the permeability, $k(\mathbf{x})$, usually exhibits complex multi-scale character [11,12]. In order to resolve the spatial correlation structures and represent the local variability accurately, the permeability is usually described using highly detailed, strongly discontinuous discrete representations [13]. Dealing with such complex models poses serious challenges to numerical flow simulation. In immiscible displacements, flow (pressure and total-velocity) and transport (saturation) are nonlinearly coupled, and that adds to the challenge. This nonlinear coupling is due to the fact that relative permeability of a fluid phase is usually represented as a strongly nonlinear function of the saturation of that phase. The relative permeability functions depend on the particular porous medium and fluid phases of interest, and they are usually obtained by performing displacement experiments on core samples.

For the domain of interest, Eq. (1) is supplemented with appropriate initial and boundary conditions. Usually, the system (reservoir) is assumed to be closed, so that no-flow boundary conditions are imposed at the periphery. Wells, which are usually represented as source/sink terms, are used to inject fluids into, or produce fluids out of, the reservoir. Since $S_w + S_o = 1$, an equivalent statement to the system of Eq. (1) is given by the following two equations:

$$-\nabla \cdot \mathbf{u} = q, \tag{4}$$

$$\phi \frac{\partial S_w}{\partial t} + \nabla \cdot (f_w \mathbf{u}) = -q_w, \tag{5}$$

where

$$\mathbf{u} = \mathbf{u}_w + \mathbf{u}_o \tag{6}$$

is the total (Darcy) velocity, and $q = q_o + q_w$. In Eq. (5), f_w is the fractional flow of water and is defined as $\mathbf{u}_w = f_w \mathbf{u}$. The total velocity can be written as

$$\mathbf{u} = -\lambda \nabla p, \tag{7}$$

where $\lambda = \lambda_w + \lambda_o$ is the total mobility, which we write as

$$\lambda = k(\mathbf{x}) \left[\frac{k_{r_w}(S_w(\mathbf{x}, t))}{\mu_w} + \frac{k_{r_o}(S_o(\mathbf{x}, t))}{\mu_o} \right]. \tag{8}$$

Note that in our case, we are ignoring capillarity and gravity, so $f_w(S_w) = \lambda_w/\lambda$, which is a (nonlinear) function of saturation only. Substitution of Eq. (7) into Eq. (4) gives the *pressure equation*:

$$\nabla \cdot \lambda \nabla p = q. \tag{9}$$

Eqs. (4) and (5) are usually referred to as the *flow* and *transport* problems, respectively. These equations are representative of the type of system that must be handled accurately and efficiently by a subsurface flow simulator. In reservoir simulation, the flow problem (Eq. (4)) is usually handled by first solving Eq. (9) for the pressure field and then computing the total velocity using Darcy's law (Eq. (7)). For immiscible two-phase problems in porous media, flow and transport form a coupled nonlinear system (Eqs. (9), (7) and (5)). The coupling is through the dependence of the total mobility field (Eq. (8)) on saturation $S(\mathbf{x}, t)$, which is a function of space and time.

Next, we describe a multiscale method for the solution of coupled multiphase flow and transport problems in highly heterogeneous porous formations.

3. Implicit multi-scale finite-volume method

The implicit MSFV approach for multi-phase flow and transport is based on the multi-scale method of Jenny et al. [10,1]. First we briefly outline the MSFV method for dealing with the flow problem, then we describe our Sequential Fully Implicit (SFI) multiscale finite-volume algorithm for coupled nonlinear flow and transport.

3.1. MSFV method for flow

Here we focus on solving the pressure equation in the presence of multiple fluid phases (Eq. (9)). This elliptic equation is of the same form as that for incompressible single-phase flow. In that case, the time-independent total mobility (Eq. (8)) is simply $\lambda = k/\mu$. As a result, the MSFV method used for single-phase flow problems [10] can be used to deal with the multi-phase pressure equation.

Without loss of generality, we describe the MSFV method for 3D orthogonal grid. Fig. 1 is a schematic of the grid, which shows eight adjacent coarse volumes (cells), $\bar{\Omega}_i$ ($i = 1, 8$), and a coarse dual volume, $\tilde{\Omega}$, obtained by connecting the cell centers of the eight coarse cells. The dual volume $\tilde{\Omega}$ is enlarged to show the underlying fine grid. The first step is to compute the fluxes across the coarse-volume interface segments, which lie inside $\tilde{\Omega}$, as a function of the surrounding coarse-volume cell-center pressures $\bar{p}$. This is achieved by constructing eight dual basis functions, $\tilde{\Phi}^i$ ($i = 1, 8$), one for each adjacent coarse cell. Each basis function is the solution of the elliptic problem

$$\nabla \cdot (\lambda \nabla p) = 0 \text{ on } \tilde{\Omega} \tag{10}$$

with the boundary condition

$$\frac{\partial}{\partial x_n} \left(\lambda \frac{\partial p}{\partial x_n} \right) = 0 \text{ on } \partial \tilde{\Omega}, \tag{11}$$
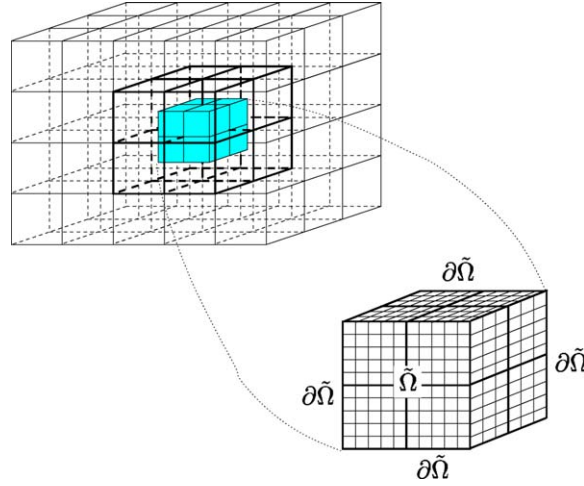
Fig. 1. 3D structured orthogonal grid with a dual control volume. The dark lines show the outline of eight adjacent coarse volumes. The dual volume obtained by connecting the cell centers of the eight coarse volumes is enlarged to show the underlying fine grid.

where x_n is the coordinate normal to the boundary of $\widetilde{\Omega}$. For dual basis function $\widetilde{\Phi}^i$, the pressure is set to zero at all corners, except at corner i where $p = 1$. The fine-scale fluxes within $\widetilde{\Omega}$ can be obtained as functions of the coarse-volume pressures $\bar{p}$ by superposition of these basis functions. Effective coarse-grid transmissibilities can then be assembled from the integral fluxes across the coarse cell interfaces. These transmissibilities can be used to solve for the global coarse grid pressure field $\bar{p}$. Note that the only approximation in the method is the local boundary condition assumption (11). For all the problems we studied to date, the multi-scale results are in excellent agreement with the fine-scale solutions.

Within a dual coarse volume, a fine-scale pressure field can be obtained using the dual basis functions as follows

$$p = \sum_{v=1}^{8} \bar{p}^v \widetilde{\Phi}^v, \tag{12}$$

where v refers to one of the eight corner vertices (centers of coarse cells). We are interested in performing transport computations of multiple phases, and it is crucial to have a flow field (pressure and velocity) that is locally conservative on the fine scale. Unfortunately, the velocity field obtained using Eq. (12) is not conservative, and that leads to mass balance errors. This is due to the fact that the fluxes across the boundaries of the dual coarse cells are not necessarily continuous. In order to reconstruct a conservative fine-scale velocity field $\mathbf{u}$ from the coarse solution $\bar{p}$, we compute an additional set of bases – the primal basis functions. Similar to the construction of the dual basis functions, an elliptic problem

$$-\nabla \cdot (\lambda \nabla p) = f \ \text{on} \ \bar{\Omega} \tag{13}$$

is solved for each primal basis function. The fine-scale fluxes extracted from the dual basis functions serve as boundary conditions for Eq. (13). To obtain a proper representation of the fine-scale velocity field in a coarse cell $\bar{\Omega}$, we ensure that: (i) the fine-scale fluxes across an interface of $\bar{\Omega}$ are continuous, and (ii) the fine-scale velocity field within $\bar{\Omega}$ satisfies

$$\nabla \cdot \mathbf{u} = \frac{\int_{\partial \bar{\Omega}} F \, \mathrm{d}\Gamma}{\int_{\bar{\Omega}} \mathrm{d}\Omega}, \tag{14}$$

where $\partial \bar{\Omega}$ is the boundary of $\bar{\Omega}$. The fine-scale flux F across $\partial \bar{\Omega}$ depends on the coarse pressures of $\bar{\Omega}$ and all adjacent coarse cells ($\bar{p}^i$, $i = 1, 27$). Therefore, the fine-scale velocity field in $\bar{\Omega}$ can be expressed as a superposition of the primal basis functions Φ^i, $i = 1, 27$.

The construction of the primal basis functions can be described as follows. Each coarse-grid pressure $\bar{p}^i$ ($i = 1, 27$) contributes to the fine-scale flux F. Therefore, each coarse pressure $\bar{p}^i$ defines the boundary

condition required to compute the fine-scale basis function Φ^i (for $i = 1, 27$). The 27 elliptic problems that must be solved are of the same size as those for the transmissibility calculations. In order to ensure solvability of these Neumann elliptic problems, we set

$$f = \frac{\int_{\partial\bar{\Omega}} F\, d\Gamma}{\int_{\bar{\Omega}} d\Omega}, \tag{15}$$

which is a uniformly distributed source term within $\bar{\Omega}$. The fine-scale pressure field within the coarse volume $\bar{\Omega}$ is given by

$$p = \sum_{j=1}^{27} \bar{p}^j \Phi^j. \tag{16}$$

The target fine-scale velocity field is reconstructed using the local fine-scale permeability and the pressure from Eq. (16). It is important to note that for incompressible flow, the computed fine-scale velocity field is divergence free.

The reconstruction of a conservative fine-scale flow field using these two sets of basis functions is elegant and computationally efficient. This is especially true for large-scale models where only a small fraction of the total number of coarse cells in the domain requires updating [1]. An alternative approach, which employs the fine-scale pressure field of Eq. (12) and avoids the use of the primal basis functions, can also be used as follows. For each (primal) coarse cell, a local problem is defined using the fluxes obtained from the fine-scale pressure field of Eq. (12) as boundary conditions. This alternative approach requires the reconstruction of a global fine-scale flow field at every time step.

However, for most problems where the fraction of dual basis functions that requires an update exceeds a small value (e.g. 5%), this alternative approach is both convenient and computationally efficient. Moreover, this alternative method allows for extending the treatment to additional flow and transport mechanisms (e.g. compressible rock and fluids, capillary pressure) in a straight forward manner.

3.2. Sequential fully implicit MSFV algorithm for coupled flow and transport

We use a sequential solution strategy in our MSFV method, where flow (pressure and total velocity) and transport (saturation) are treated separately and differently. The algorithms are specialized to the specific characteristics of the governing equations. In our Sequential Fully Implicit (SFI) MSFV algorithm, each time step consists of an outer loop to solve the coupled problems of flow and transport, and an inner (nonlinear) Newton loop to solve the implicit transport problem given the updated flow field.

A flow diagram of the outer loop for one time step is shown in Fig. 2. The superscripts n and ν denote the old time and iteration levels, respectively. Saturation is represented by S, the total velocity field by $\mathbf{u}$, the computation of the pressure field by the operator P, and the computation of the transport problem (i.e. saturation field) by T. For each outer iteration, using the total-mobility field we solve the pressure equation (Eq. (9)), which is operator P in Fig. 2, and we compute (reconstruct) the fine-scale total-velocity field. This step is obtained using the MSFV method outlined in the previous subsection and explained in detail by Jenny et al. [10]. Specifically, we solve

$$\nabla \cdot k \left[\frac{k_{r_w}(S_w^\nu)}{\mu_w} + \frac{k_{r_o}(S_w^\nu)}{\mu_o} \right] \nabla p^{\nu+1} = q \tag{17}$$

for $p^{\nu+1}$, and we update the total velocity field, $\mathbf{u}^{\nu+1}$. Now, given $\mathbf{u}^{\nu+1}$, a second, or inner, Newton loop is used to solve the saturation equation for the current time step implicitly, (operator T in Fig. 2). The semi-discrete form of the saturation equation is given by

$$\phi \frac{S_w^{\nu+1} - S_w^n}{\Delta t} + \nabla \cdot (f_w^{\nu+1} \mathbf{u}^{\nu+1}) = -q_w \tag{18}$$
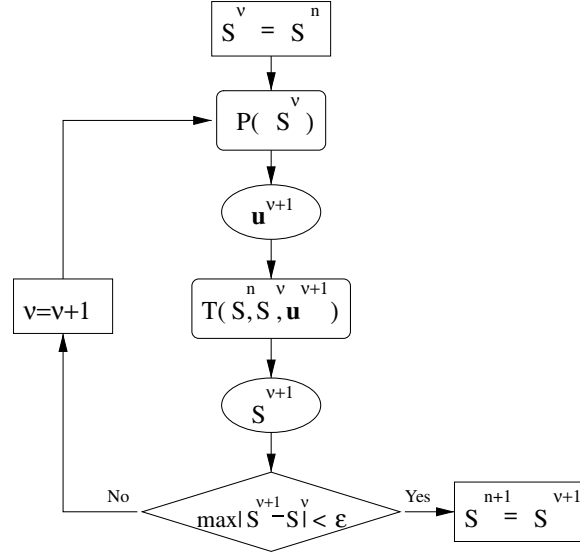
with

Fig. 2. Flow diagram of the sequential fully implicit MSFV scheme. *P* and *T* are operators for the computation of the pressure field and the transport problem, respectively.

$$f_{\mathrm{w}}^{\nu+1} = \left(\frac{\lambda_{\mathrm{w}}}{\lambda}\right)^{\nu+1} = \frac{Mk_{\mathrm{r_w}}\left(S_{\mathrm{w}}^{\nu+1}\right)}{Mk_{\mathrm{r_w}}\left(S_{\mathrm{w}}^{\nu+1}\right) + k_{\mathrm{r_o}}\left(S_{\mathrm{w}}^{\nu+1}\right)},\tag{19}$$

where $M = \mu_{\mathrm{o}}/\mu_{\mathrm{w}}$ is the viscosity ratio. The hyperbolic saturation equation (Eq. (18)) is amenable to solution using a local scheme, such as the overlapping Schwarz method. The primal coarse grid provides a natural blocking structure, and we apply the iterative Schwarz method block wise (that is, each block consists of the fine-grid in a primal coarse cell). We use a simple first-order upwinding scheme, where the fine-grid saturations from the neighboring coarse cells (evaluated at the previous iteration level) serve as boundary conditions. Our experience indicates that implicit solution of the saturation equations using this approach is quite robust and computationally efficient. Once the saturation field is converged (to within a small tolerance) everywhere, the new saturation distribution is used to update the total-mobility field (Eq. (8)), which is used in the construction of the elliptic pressure system employed in the next outer iteration.

We experimented with various coupling schemes. Our results for a wide range of strongly heterogeneous nonlinear two-phase problems indicate that it is quite important to have a total-velocity field that is conservative on the fine-scale for each outer iteration. The conservation property is not only important for obtaining accurate and robust implicit solutions of the saturation equations in the inner Newton loop, it is also crucial for having a coupling scheme of nonlinear flow and transport that is both reliable and computationally efficient. This is especially the case for large time step sizes.

Various tolerance criteria may be used to control the outer loop iteration, that is, the repeated two-stage solution of the pressure and saturation equations. We have used criteria based on maximum saturation change as well as the ratio of the total-mobility obtained from two consecutive iterations. This is an area of ongoing investigation. In our sequential fully implicit multiscale approach, SFI-MSFV, if a single iteration of the outer loop is followed by explicit integration of the saturation equations, we obtain the IMPES-based MSFV method [1]. On the other hand, if only a single outer loop iteration is performed, we obtain a sequential implicit MSFV method. The sequential implicit formulation [14–16] has proved quite effective in reservoir simulation practice. It is not unconditionally stable, however. Moreover, the sequential implicit scheme is not exactly conservative for all fluid phases [17,16].

The plot in Fig. 3, which shows the convergence history of a typical time step, demonstrates that only few iterations are required to achieve convergence. The SFI-MSFV method has been tested for very large heterogeneous multiphase problems, and the coupling scheme has proved to be quite robust even for very large time steps (i.e. high throughput).
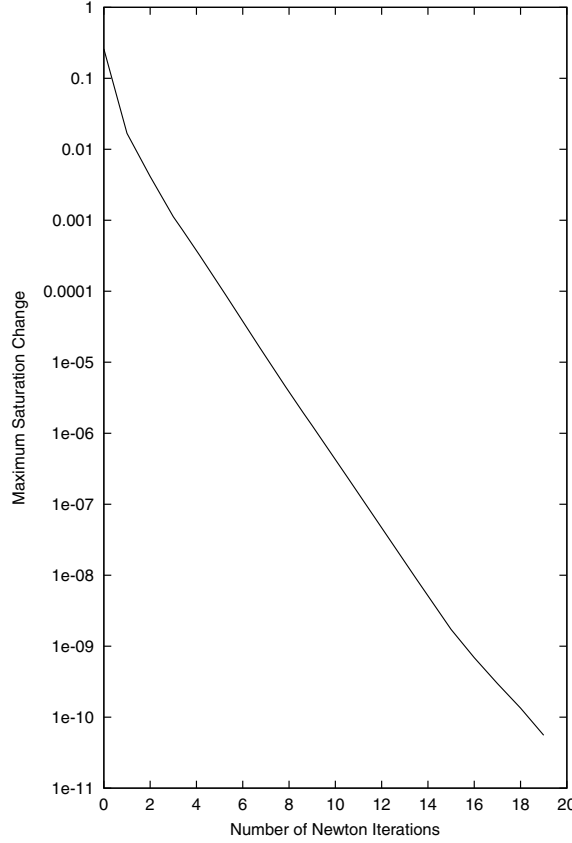
Fig. 3. Coupling between the pressure and the saturation equation. Convergence history of a typical time step.

3.3. Adaptive computation

The most expensive part of the SFI-MSFV algorithm is the reconstruction of the dual and primal basis functions. Therefore, to obtain higher efficiency, it is desirable to recompute them only when and where it is absolutely necessary. We employ the scheme that was developed to adapt the flow computations of the IMPES-based MSFV method [1]. Namely, if the condition

$$\frac{1}{1 + \epsilon_\lambda} < \frac{\lambda^v}{\lambda^{v-1}} < 1 + \epsilon_\lambda \qquad (20)$$

is not fulfilled (the superscripts v and $v - 1$ denote the previous two iterations and $\epsilon_\lambda > 0$ is a user defined value) for all fine cells inside a coarse dual cell, then the dual basis functions of that control volume have to be reconstructed. An illustration of this scheme in 2D is shown in Fig. 4, where the fine and the coarse grids are drawn with thin and bold lines, respectively. The black squares represent the fine cells in which condition (20) is not fulfilled. The squares with bold dashed lines are the control volumes for which the dual basis functions have to be reconstructed. The shaded regions represent the coarse cells for which the primal basis functions must be updated. In the schematic 2D example of Fig. 4, only 32 of 420 (4 for each of the 105 coarse grid nodes) total dual basis functions and 207 of 756 (9 for each of the 84 coarse cells) total primal basis functions have to be reconstructed. Of course, these numbers depend heavily on the user defined threshold ϵ_λ. In general, a smaller threshold triggers more fine cells, and as a consequence more basis functions are recomputed each time step. For a wide variety of test cases, we found that taking ϵ_λ to be <0.2 yields marginal changes in the obtained results. In the SFI-MSFV method, the fraction of coarse cells that require updating of the basis functions is typically higher than that observed for the IMPES-based MSFV scheme, and that is expected.
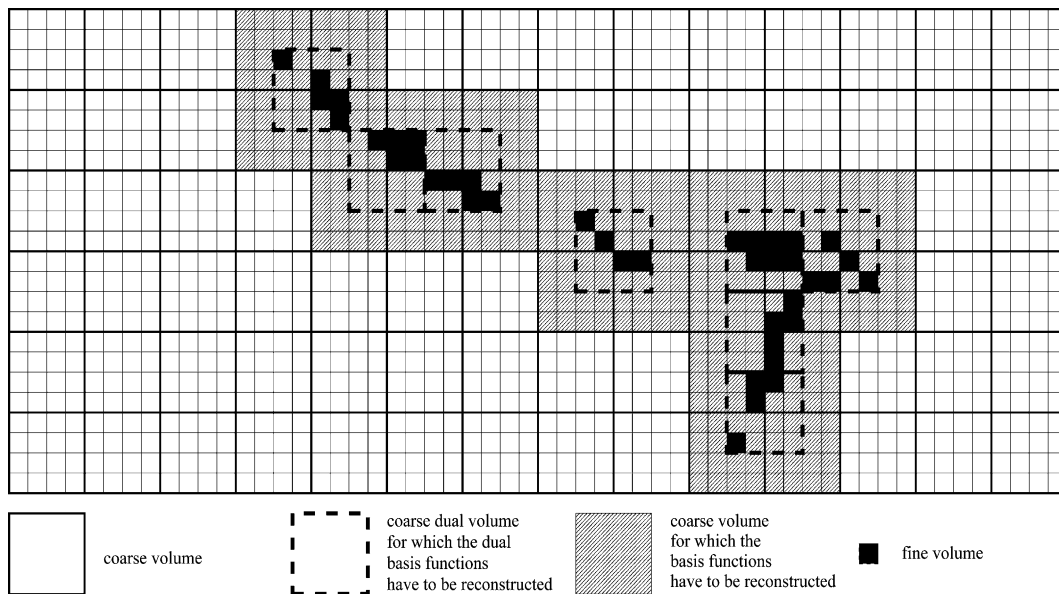
Fig. 4. Illustration of the adaptive scheme to update the basis functions selectively. The fine and coarse grids are represented by thin and bold lines, respectively. The black squares mark the fine cells in which condition (20) is not fulfilled. The control volumes in which the dual basis functions must be updated are drawn with bold dashed lines, and the shaded regions are those in which the primal basis functions must be reconstructed.

However, we have observed that for reasonably large time steps, the fraction of bases functions that must be recomputed rarely exceeds 20%.

As noted at the end of Section 3.1, one can avoid using the primal basis functions by computing the total velocity directly using the pressure field computed with the help of the dual basis functions. This can also lead to significant savings especially if the fraction of coarse volumes requiring an update is much greater than 5%. We finally mention that taking advantage of adaptive computation in the inner Newton loop of our coupling scheme (where implicit solution of the saturation equations is performed) is much more challenging than that for an IMPES-based scheme where an explicit scheme is used to integrate the saturation equation.

4. Numerical results

Recently, the MSFV method combined with an IMPES scheme was tested for two-phase flow and transport in a heterogeneous 3D model with more than 140,000 cells, and it was demonstrated that the multi-scale results are in excellent agreement with reference fine-scale solutions [1]. Moreover, that MSFV method was shown to be significantly more efficient than an established Multi-Purpose Reservoir Simulator (MPRS). However, in cases with severe permeability heterogeneity, the computational efficiency of the overall scheme can be compromised due to the restrictions on the time step size inherent in the IMPES scheme. Here we demonstrate how this problem is resolved by applying our sequential fully implicit (SFI) MSFV method. The objective of the numerical studies is to show the following:

(1) The results obtained with the SFI-MSFV method are in excellent agreement with reference fine-scale results.
(2) The results obtained with the multiscale method are not very sensitive to the choice (size) of the coarse grid.
(3) The sequential fully implicit coupling scheme leads to robust behavior even for large time step sizes.
(4) The SFI-MSFV approach is computationally efficient.

To compute fine-scale reference solutions, an established Multi-Purpose Reservoir Simulator (MPRS) was used. The MPRS simulator is based on a generalized compositional formulation and is capable of modeling a wide range of reservoir displacement processes. In the MPRS simulator, a simultaneous solution method of the conservation equations is used for the fully implicit formulation; moreover, the MPRS simulator offers an IMPES capability. Sophisticated algorithms for both the nonlinear and linear loops are implemented in this state-of-the-art reservoir simulator. It has to be mentioned that the efficiency of both MPRS and MSFV simulations depends on the choice of various parameters, which can be further optimized. Consequently, a detailed quantitative performance comparison is not the objective. Instead, in this section we want to demonstrate that a multiscale finite-volume framework carries the promise of solving highly heterogeneous, large-scale reservoir simulation problems of practical interest in a robust and computationally efficient manner. In the next subsection, the test cases are described; Section 4.2 addresses items (1) and (2) and Section 4.3 deals with items (3) and (4).

4.1. Test cases

To study the accuracy and efficiency of the SFI-MSFV algorithm, 2D and 3D test cases with uniformly spaced orthogonal 60×220 and $60 \times 220 \times 85$ grids were used. The 3D grid and permeability field are obtained from the SPE 10 test case [18], which is known to be an extremely difficult problem for reservoir simulators. While the 3D test case was used for computational efficiency assessment, 2D test cases, which consist of the top and bottom layers of the SPE 10 model, are used to demonstrate the accuracy of the SFI-MSFV method. Fig. 5 shows the permeability field with a water injector in the center and four producers wells in the corners. These well locations are used for all the following studies. The reservoir is initially fully saturated with oil. We take $M = \mu_o / \mu_w = 10$, and use quadratic relative permeability curves (i.e. $k_{r_w} = S_w^2$ and $k_{r_o} = (1 - S_w)^2$). These choices lead to a nonlinear coupling of flow and transport, and that is an essential feature of reservoir simulation problems of practical interest.

4.2. 2D simulations of the top and bottom layers

Our SFI-MSFV simulator does not have a sophisticated well model. Accommodating the presence of wells in the MSFV framework requires special treatment, including the construction of well-specific basis functions [19]. Here, wells are modeled by defining the total rates for each perforated coarse cell. Therefore, in order to
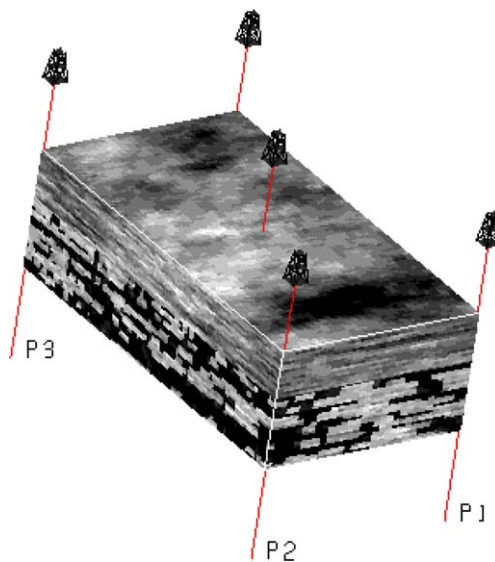

Fig. 5. 3D test case: permeability field of the SPE 10 problem (darker means lower permeability).

make accuracy comparisons rigorous, each fine-grid cell in the MPRS simulations, which is inside a perforated coarse cell, becomes a well (i.e. a source/sink term) with a constant total rate. For large 3D models, this poses a technical problem since MPRS is not designed to handle an arbitrarily large number of individual wells. For this reason we decided to do the accuracy assessment in 2D, i.e. with the top and the bottom layers of the 3D model. These two layers, for which the permeability fields are shown in Fig. 6, are representative for the two characteristically different regions of the full model. We performed MSFV simulations with uniformly spaced 10×22 and 20×44 coarse grids and compared the results with the fine-scale solution on a 60×220 grid. As in the full 3D test case, there are four producers at the corners which are distributed over an area of 6×10 fine-scale volumes. The injector is located in the center of the domain and is distributed over an area of 12×20 fine-scale volumes. The rates are the same for all fine-scale volumes (positive for the producer volumes and negative for the injector volumes). In Figs. 7 and 8, the computed saturation fields are shown after 0.093 PVI for the bottom and top layers, respectively. The rightmost plots in these figures show the fine-scale reference solutions; the left and center plots show the MSFV results for 10×22 and 20×44 coarse grids, respectively. It can be observed for both layers that the agreement is excellent, and that the multi-scale method is not sensitive to the choice (size) of the coarse grid. More quantitative comparisons are shown in Fig. 9 where the fine-scale and multi-scale oil cut (fraction of fluid produced that is oil) and cumulative recovery curves are plotted. Considering the difficulty of these test problems and the fact that two independently implemented simulators are used for the comparisons, this agreement is remarkable.

4.3. 3D simulations

While 2D studies are appropriate to study the accuracy of the sequential fully implicit MSFV method, 3D computations for highly detailed models with strong permeability heterogeneity are required for a meaningful assessment of the computational efficiency. We employed the 3D test case (i.e. the SPE 10 permeability field) described above. A coarse $10 \times 22 \times 17$ grid (shown in Fig. 10) was used and 0.5 pore volumes were injected. Unlike the SFI-MSFV simulations, the wells for the MPRS simulations were defined on the fine-grid.
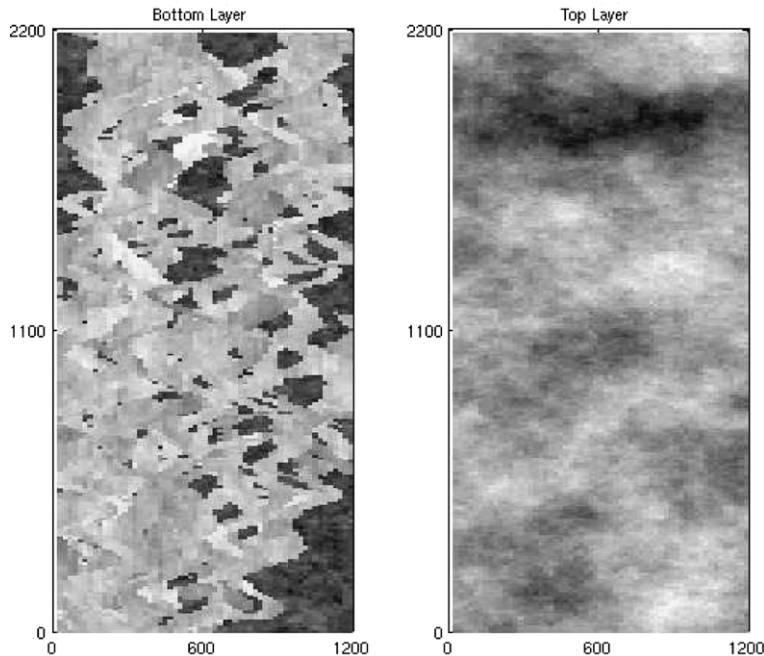

Fig. 6. Permeability fields of the bottom (left) and top (right) layers (darker means lower permeability). These two layers are representative for the two characteristically different regions of the full 3D model.
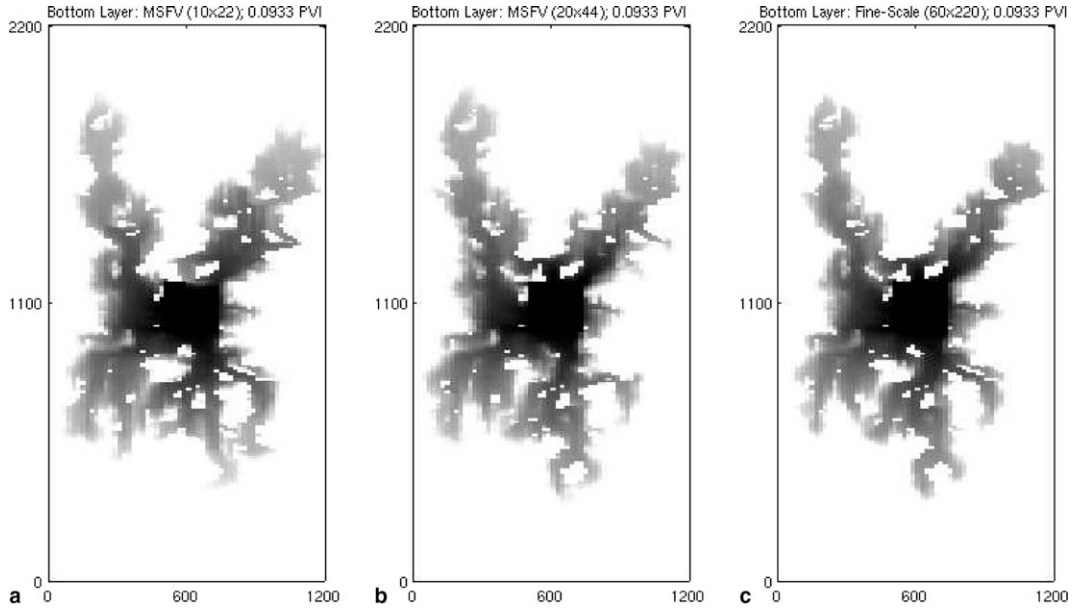
Fig. 7. The saturation fields (dark is water) from three different simulations of the bottom layer of SPE 10.
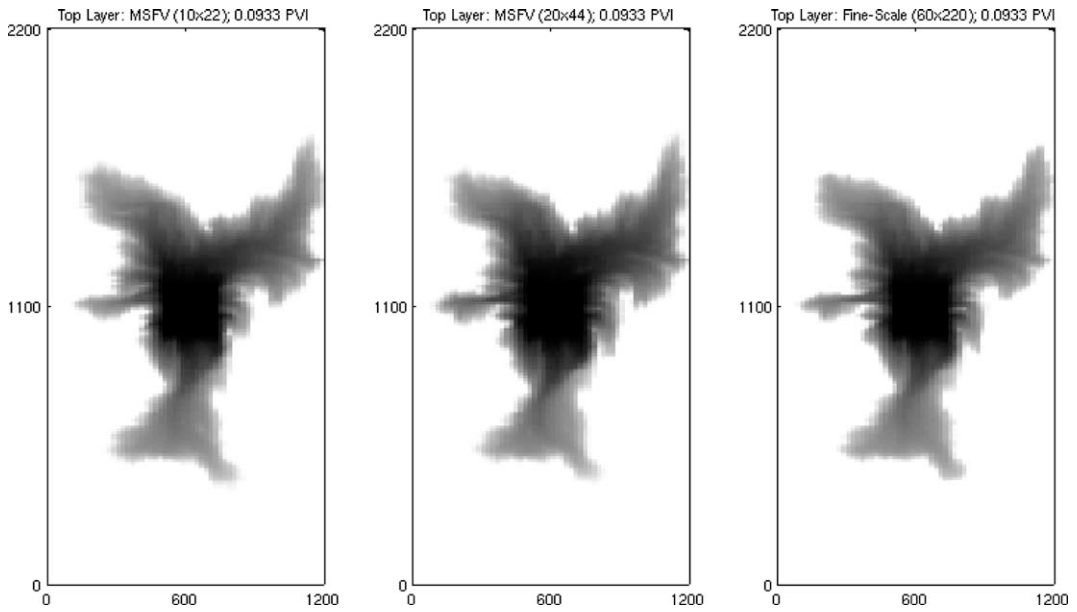

Fig. 8. The saturation fields (dark is water) from three different simulations of the top layer of SPE 10.

Table 1 shows an example of the computational time and the required number of time steps for SFI-MSFV and MPRS simulations. The table shows that the implicit MSFV method is significantly faster than MPRS. We mention here that although MPRS uses an elaborate control algorithm for time step selection, we invested a significant effort so that the MPRS simulations are as fast as possible for this extremely difficult and stiff problem. That required balancing several factors (over the injection period of 0.5 pore volumes) including the number of time steps and the average number of Newton iterations per time step. On the other hand, with the SFI-MSFV method, we fixed the time step size at a constant value. The choice was guided by accuracy considerations since we were able to take time steps that are much larger than was possible with MPRS.
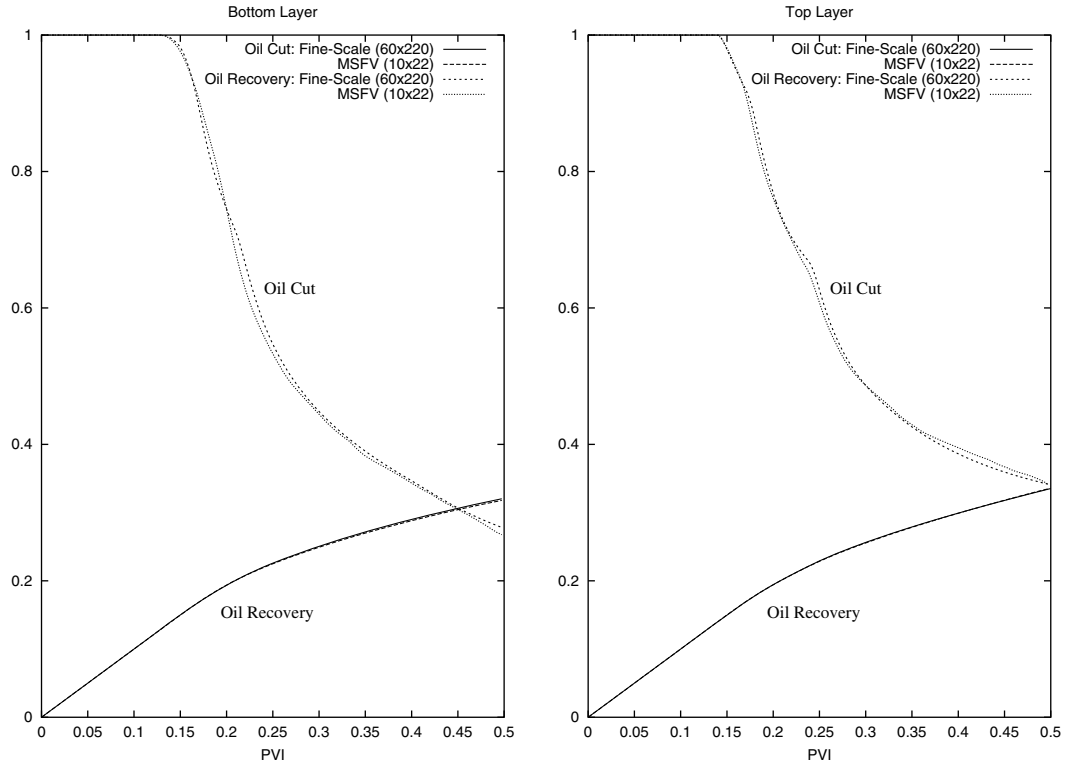
Fig. 9. Oil cut and recovery curves for the bottom and top layers of the SPE 10 problem.
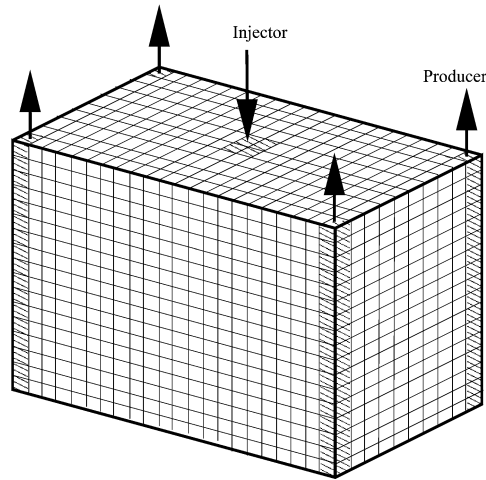

Fig. 10. 3D test case: coarse $10 \times 22 \times 17$ grid with wells.

Fig. 11 shows the oil cut and recovery curves obtained with multi-scale simulations using 50 and 200 time steps. The close agreement between the results indicates that the accuracy of the computed flow response is not strongly sensitive to the time step size used. The sequential fully implicit coupling scheme allows for specializing the solution methods to the flow and transport components, which seems to improve the robustness of the outer and inner nonlinear loops with respect to the time step size. This is an area of ongoing research. Finally, for a number of highly heterogeneous systems, we have observed that the cost of MSFV simulation

Table 1
Efficiency comparisons between SFI-MSFV and MPRS simulations for the SPE 10 permeability field, which has $60 \times 220 \times 85$ cells

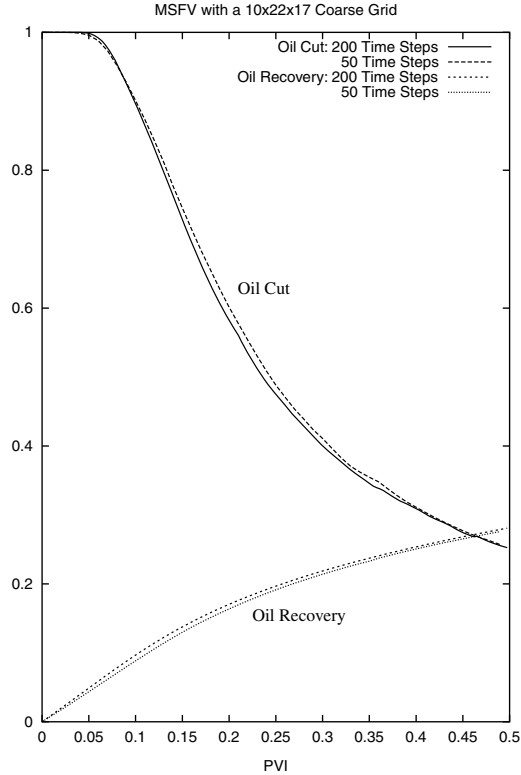| Simulator	CPU time (min)	Time steps	Recomputed basis functions (%)	Coarse pressure computations (%)
MPRS	3325	790		
MSFV	297	200	10	98

A coarse $10 \times 22 \times 17$ grid was used for the MSFV computations.

Fig. 11. Oil cut and oil recovery.

scales almost linearly with problem size, and since the dual and primal basis functions can be computed independently (and adaptively), the method is ideally suited for parallel computations and large-scale problems of practical interest.

5. Conclusions

An adaptive sequential fully implicit multi-scale finite-volume (SFI-MSFV) method for 3D nonlinear multi-phase flow and transport in heterogeneous porous media was developed and tested for various difficult test cases. The method has proved to be very efficient, and the results are in excellent agreement with reference fine-scale solutions. While the discussion here was limited to incompressible nonlinear two-phase flow, the method is equally applicable to three-phase flow. In that case, one must solve two saturation equations implicitly in the inner loop of the coupling scheme.

The multiscale finite-volume (MSFV) framework is very promising, and there is a significant ongoing effort to extend the modeling capability in several areas. These include: (1) coupled well models, (2) highly compressible fluids and rock, (3) solubility effects including saturated (free gas phase) and under-saturated conditions (no free gas phase), and (4) the black-oil model (i.e. three component, three-phase, nonlinear compressible

flow). Finally, numerical issues related to severe anisotropy in both the grid and the underlying permeability field pose an interesting challenge and is an active research area.

Acknowledgment

References

[1] P. Jenny, S.H. Lee, H.A. Tchelepi, Adaptive multiscale finite volume method for multi-phase flow and transport, Multiscale Model. Simul. 3 (2005) 50–64.

[2] L.J. Durlofsky, Numerical calculation of equivalent grid block permeability tensors for heterogeneous porous media, Water Resour. Res. 27 (1991) 699–708.

[3] L.J. Durlofsky, R.C. Jones, W.J. Milliken, A nonuniform coarsening approach for the scale up of displacement processes in heterogeneous porous media, Adv. Water Resour. 20 (1997) 335–347.

[4] Y. Gautier, M.J. Blunt, M.A. Christie, Nested gridding and streamline-based simulation for fast reservoir performance prediction, Comput. Geosci. 3 (1999) 295–320.

[5] T. Hou, X.H. Wu, A multiscale finite element method for elliptic problems in composite materials and porous media, J. Comp. Phys. 134 (1997) 169–189.

[6] Z. Chen, T.Y. Hou, A mixed multiscale finite element method for elliptic problems with oscillating coefficients, Math. Comput. 72 (2003) 541–576.

[7] T. Arbogast, Implementation of a locally conservative numerical subgrid upscaling scheme for two phase darcy flow, Comput. Geosci. 6 (2002) 453–481.

[8] T. Arbogast, S.L. Bryant, A two-scale numerical subgrid technique for waterflood simulations, Soc. Petrol. Eng. J. (2002) 446–457.

[9] J.E. Aarnes, On the use of a mixed multiscale finite element method for greater flexibility and increased speed or improved accuracy in reservoir simulation, Multiscale Model. Simul. 2 (3) (2004) 421–439.

[10] P. Jenny, S.H. Lee, H.A. Tchelepi, Multi-scale finite-volume method for elliptic problems in subsurface flow simulation, J. Comput. Phys. 187-1 (2003) 47–67.

[11] R.J. Hoeksema, P. Kitanidis, Analysis of the spatial structure properties of selected aquifers, Water Resour. Res. 21 (4) (1985) 563–572.

[12] G. Dagan, Flow and Transport in Porous Formations, Springer, New York, NY, 1989.

[13] C. Deutsch, Geostatistical Reservoir Modeling, Oxford University Press, New York, NY, 2002.

[14] A.G. Spillette, J.G. Hillestad, H.L. Stone, A high-stability sequential solution approach to reservoir simulation, SPE 4542, Presented at the 48th Annual Fall Meeting of SPE of AIME, Las Vegas, NV, September 30–October 3, 1973.

[15] K.H. Coats, W.D. George, C. Chu, B.E. Marcum, Three-dimensional simulation of steamflooding, Soc. Petrol. Eng. J. (1974) 573–592.

[16] J.W. Watts, A compositional formulation of the pressure and saturation equations, Soc. Petrol. Eng. Reservoir Eng. (1986) 243–252.

[17] K. Aziz, A. Settari, Petroleum Reservoir Simulation, Applied Science Publishers, London, England, 1979.

[18] M.A. Christie, M.J. Blunt, Tenth SPE comparative solution project: A comparison of upscaling techniques, SPE Reserv. Eval. Eng. 4 (2001) 308–317.

[19] C. Wolfsteiner, S.H. Lee, H.A. Tchelepi, Well modeling in the multiscale finite volume method for subsurface flow simulation, Multiscale Model. Simul. (under review), September 2005.